AAS 15-690

ORBIT STABILITY OF OSIRIS-REX IN THE VICINITY OF BENNU USING A HIGH-FIDELITY SOLAR RADIATION MODEL

Trevor W. Williams,[*] Kyle M. Hughes,[†]
Alinda K. Mashiku[‡] and James M. Longuski[§]

Solar radiation pressure is one of the largest perturbing forces on the OSIRIS-Rex trajectory as it orbits the asteroid Bennu. In this work, we investigate how forces due to solar radiation perturb the OSIRIS-REx trajectory in a high-fidelity model. The model accounts for Bennu's non-spherical gravity field, third-body gravity forces from the Sun and Jupiter, as well as solar radiation forces acting on a simplified spacecraft model. Such high-fidelity simulations indicate significant solar radiation pressure perturbations from the nominal orbit. Modifications to the initial design of the nominal orbit are found using a variation of parameters approach that reduce the perturbation in eccentricity by a factor of one-half.

INTRODUCTION

For several phases in the Origins Spectral Interpretation Resource Identification Security Regolith EXplorer (OSIRIS-Rex) mission, the spacecraft is subject to strong solar radiation pressure (SRP) perturbations that degrade the stability of the orbit and may interfere with mission proximity operations. This paper presents the analysis done to model the SRP forces, using a numerical method known as ray tracing, and compares the orbit stability to a "cannonball" SRP model. We also perform a study to design a stable orbit that minimizes the evolution of the eccentricity.

The Osiris-REx Mission

OSIRIS-REx is a sample return mission to the near-Earth asteroid Bennu (also known as 1999 RQ36). The mission is part of NASA's New Frontiers Program and is set to launch in 2016, arrive at Bennu in 2018, and return a sample to Earth in 2023. Bennu is a carbonaceous asteroid and contains original material form the solar nebula (the nebula from which our Solar System

[*] Aerospace Engineer, Navigation and Mission Design Branch, NASA Goddard Space Flight Center, 8800 Greenbelt Road, Greenbelt, Maryland 20771, U.S.A. E-mail: trevor.w.williams@nasa.gov. AIAA Associate Fellow.
[†] Doctoral Candidate, School of Aeronautics and Astronautics, Purdue University, 701 W. Stadium Avenue, West Lafayette, Indiana 47907, U.S.A. E-mail: kylehughes@purdue.edu. AIAA Student Member.
[‡] Aerospace Engineer, Navigation and Mission Design Branch, NASA Goddard Space Flight Center, 8800 Greenbelt Road, Greenbelt, Maryland 20771, U.S.A. E-mail: alinda.k.mashiku@nasa.gov.
[§] Professor, School of Aeronautics and Astronautics, Purdue University, 701 W. Stadium Avenue, West Lafayette, Indiana 47907, U.S.A. E-mail: longuski@purdue.edu. AAS Member, AIAA Associate Fellow.

formed). The OSIRIS-REx mission will thoroughly characterize Bennu to address many of the NASA Solar System Exploration Objectives, and give insight to the origin of water and organic material on Earth as well as the origin of the Solar System itself. Additionally, understanding the physical and chemical properties of Bennu may prevent a future collision with Earth. Since Bennu crosses the Earth's orbit, there is a risk of a future impact and the data collected by OSIRIS-REx will be essential for future scientists and engineers to develop a mission to prevent such an impact.[1,2]

Previous missions have identified that SRP forces are a significant perturbation. (One such example being the Galileo mission.[3]) For spacecraft orbiting small bodies, such as OSIRIS-REx, the perturbations are expected to be even more significant, due to the comparatively small gravity force of the central body. With the understanding that the SRP forces are the most prominent perturbations for OSIRIS-REx, we investigate a method to accurately model and capture these perturbations.

Solar Radiation Pressure Forces

Solar radiation pressure is the force per unit area due to sunlight "pushing" on an object—that object (in this case) being the OSIRIS-REx spacecraft. The interaction itself is due to the momentum transfer that results from the Sun's photons colliding with the spacecraft surface. The result is a net force acting on the spacecraft due to SRP, which will perturb the spacecraft's trajectory (and orientation).

SRP is characterized by

$$P_{SRP} = \frac{K\Phi}{c\, R_{AU}} \tag{1}$$

where K is the fraction of the Sun visible to the spacecraft (i.e. the fraction that is not eclipsed by any other body), Φ is the solar flux (or total solar irradiance in units of W/m^2) at 1 AU, c is the speed of light, and R_{AU} is the Sun-spacecraft distance in units of AU.

When sunlight contacts the spacecraft surface it is absorbed, reflected specularly or reflected diffusely, or some combination of these three, with the relative amounts determined by the material properties of the spacecraft surface. Each type imparts a force on the spacecraft, and the net force on the spacecraft due to SRP is the sum of the net forces due to absorbed and reflected light.

The force on a flat plate due to absorbed light is illustrated Figure 1. In the figure, $\hat{S}$ is the unit vector pointed at the Sun, $\widehat{N}$ is the area unit normal of the flat plate, θ is the angle between the two unit vectors, A is the area of the plate, and $\vec{F}_a$ is the force on the plate due to absorbed light. The force is directed opposite $\hat{S}$ and is computed by

$$\vec{F}_a = -P_{SRP} C_a A \cos\theta\, \hat{S} \tag{2}$$

where C_a is the fraction of light that is absorbed on the plate (determined from the plate's material properties). The $A\cos\theta$ term represents the amount of plate area as "seen" by the Sun. For example, in the extreme case with $\theta = 90^o$, the Sun would merely see the plate as a vertical

edge, and thus no interaction between the light and the plate would occur at all, and (as expected) the force $\vec{F}_a$ would be zero.

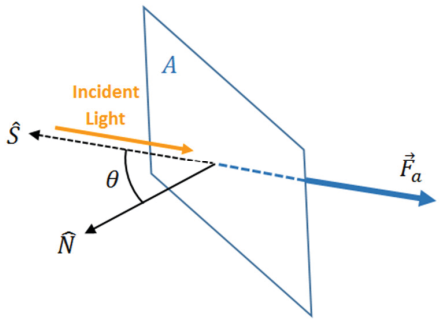

Figure 1. Force due to absorbed light is in the direction opposite the Sun.

The forces due to reflected light are illustrated in Figure 2 for specular and diffuse reflection. For specular reflection, the force component due to the incident light is essentially the same as that for absorbed light. A force of identical magnitude then also results due to the reflected light, but in the direction opposite the reflected ray (as shown in the figure). Using vector addition with the forces due to incident and specularly reflected light, the components in the plane of the plate cancel out (due to symmetry) and the components normal to the plate are doubled. The resulting sum is the force due to specular reflection given by

$$\vec{F}_s = -2P_{SRP}C_sA\cos^2\theta\,\hat{N} \tag{3}$$

where C_s is the fraction of light that is specularly reflected.

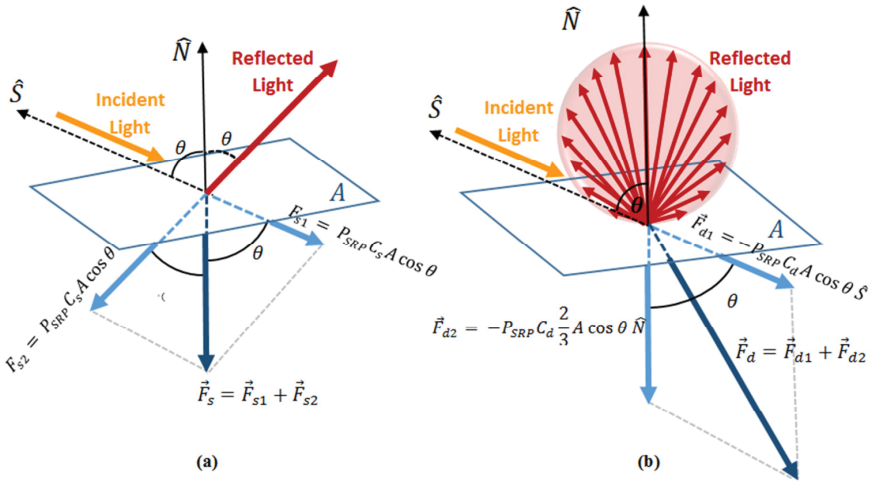

Figure 2. Specular (a) and diffuse (b) reflection forces on a flat plate.

The force due to diffuse light is slightly more complicated. The component in the $\hat{S}$ direction is purely due to the incident light. The force component normal to the plate is found using the

Lambert law,[3–5] which assumes the reflected light diffuses spherically outward (as shown in Figure 2). More precisely this assumes that the intensity of light is greatest along the $\hat{N}$ direction, and then drops off (in magnitude) with the cosine of the angle between the reflected light ray and $\hat{N}$. The end result is all force components (due to each reflected ray) in the plane of the plate cancel out (due to symmetry). In the normal direction, net force components sum to 2/3 of the magnitude of the force due to incident light (i.e. $\frac{2}{3}F_{d1}$). (See Refs 3–5 for the full derivation.) Thus, the net force due to diffusely reflected light is given by

$$\vec{F}_d = -P_{SRP}C_d A\cos\theta\left(\hat{S} + \frac{2}{3}\hat{N}\right) \tag{4}$$

where C_d is the fraction of light that is reflected diffusely. We note that since all light considered in this model is absorbed, reflected specularly, or reflected diffusely,

$$C_a + C_s + C_d = 1. \tag{5}$$

Using this equation, the force due to absorbed light can be rewritten in terms of C_s and C_d, given by

$$\vec{F}_a = -P_{SRP}(1 - C_s - C_d)A\cos\theta\,\hat{S}. \tag{6}$$

The net force due to SRP on the spacecraft is therefore

$$\begin{aligned}\vec{F}_{SRP} &= \vec{F}_a + \vec{F}_s + \vec{F}_d \\ &= -P_{SRP}A cos\theta\left\{(1 - C_s)\hat{S} + 2\left(C_s cos\theta + \frac{1}{3}C_d\right)\hat{N}\right\}.\end{aligned} \tag{7}$$

Similar derivations of the SRP force can be found by Longuski et al.,[3] Ziebart,[5] Georgevic,[6] Wertz,[7] Vallado,[8] and several other references.

The Cannonball Model

A very commonly used method for simplifying the SRP model is to assume the spacecraft is a perfect sphere. This spherical SRP model is often referred to as the cannonball model. The traditional cannonball SRP model accounts somewhat for reflected light, but only in the Sun direction. To simplify the SRP model in Eq. (7) to the cannonball SRP model, we assume the spacecraft is a perfect sphere. An immediate consequence of this is that both vector components from Eq. (7) are in the $\hat{S}$ direction, and the angle $\theta = 0$. The result is

$$\vec{F}_{SRP} = -P_{SRP}A_{cb}C_R\hat{S} \tag{8}$$

where A_{cb} is the circular cross-sectional area of the "cannonball" (typically set to a value on the order of the true spacecraft's area as seen by the Sun). The value C_R (called the "reflectivity") is a number between 0 and 2 and is a property of the spacecraft surface material. By using Eq. (7) on a perfect sphere, and putting the result into the form of Eq. (8), the reflectivity can be expressed as

$$C_R = 1 + C_s + {}^{2}/_{3}\,C_d\,. \tag{9}$$

HIGH FIDELITY SRP FORCE MODELING USING RAY TRACING

Ray Tracing

Ray tracing is the process of following (or "tracing out") the path of a light ray as it absorbs and reflects off various surfaces on the spacecraft. Light rays that are reflected can move on to encounter many more surfaces, which will result in more reflections and may result in more subsequent encounters. In this study, only the specularly reflected light is considered for subsequent encounters. The forces for all encounters are then computed using Eq. (7) and summed over the entire spacecraft. The ray-tracing algorithm is implemented via the Goddard Space Flight Center's (GSFC's) in-house Solar Pressure and Aerodynamic Drag (SPAD) program, which is discussed in more detail in the next section.

Solar Pressure and Aerodynamic Drag (SPAD) Tool

The SPAD analysis tool is a GSFC in-house tool for computing SRP and drag forces on a spacecraft. For Orbit B of the OSIRIS-REx trajectory, drag forces are not considered for analysis (as would be expected), therefore the following discussion only addresses the SRP analysis capabilities of the SPAD program.

Before any SRP analysis can be done in SPAD, a spacecraft model must be generated. The SPAD program contains tools to create a surface model of a spacecraft using simple shapes (flat plates, spheres, prisms, cones, etc.), and to specify material properties (i.e. C_a, C_s, and C_d) for each surface. For this analysis, a simple model of OSIRIS-REx is built in SPAD, and is shown in Figure 3. The material properties used for each surface on the spacecraft are given by Olds.[9] With the spacecraft model built, the SRP analysis can be done in SPAD via the ray-tracing algorithm.

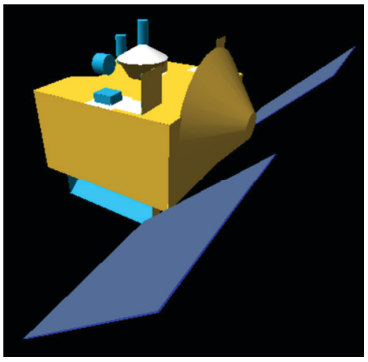

Figure 3. OSIRIS-REx spacecraft model built using SPAD. Each color shown represents a different material with a unique set of properties.

The following describes the SPAD program's algorithm for modeling ray tracing, which is very similar to that described in detail by Ziebart.[5]

Creating the Pixel Array

A plane is created in space such that its normal vector is directed at the origin of the spacecraft's body-fixed frame. This normal vector represents the direction that light is emitted from the Sun

onto the spacecraft (as if the light is emitted from the plane). The opposite of the plane's normal vector provides the Sun direction, $\hat{S}$. The $\hat{S}$ vector, and therefore the orientation of the plane, can be specified in the spacecraft's body-fixed frame, by a given azimuth and elevation angle (chosen by the user).

The size of the plane is chosen such that (when projected normally outwards) it encompasses the entire spacecraft. (See Figure 4.) The plane is then divided into a square grid of pixels (creating an array), and a vector (representing a light ray) is placed at the center of each pixel. These light-ray vectors are directed such that they are parallel to the surface normal of the plane. The pixel size (i.e. the array resolution) is user defined, and is specified by stating the (uniform) distance between adjacent light-ray vectors.

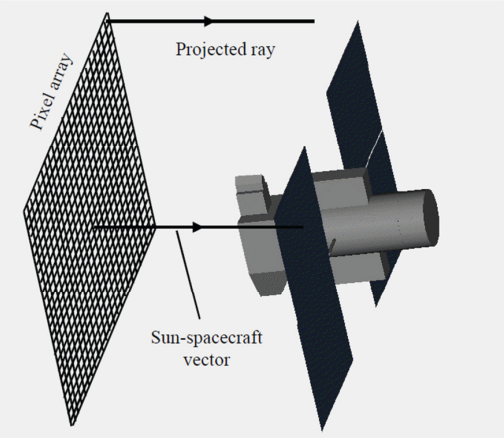

Figure 4. Ray Tracing implementation illustrating the projected rays from the pixel array unto the spacecraft (Ziebart[10]).

Typically, the space about the spacecraft is discretized into a set of azimuth and elevation angles (specified in SPAD), and a pixel array is created for each—representing light emitted onto the spacecraft (in discretized space) for all spacecraft orientations. Interpolation is used for computing SRP at intermediate azimuth and elevation angles.

The vector at the center of each pixel represents a light ray and is part of the light-ray model. Each light-ray model consists of the vector position and direction, and the pixel area. The positions of each light ray vector as well as the (square) pixel area are computed from the specified pixel size.

Projecting each Light Ray onto the Spacecraft Model

Each light-ray vector is projected onto the spacecraft model. All intersections between a light-ray and the spacecraft model are computed, however only the intersection closest to the pixel array is considered (i.e. assuming an opaque spacecraft surface, only the nearest intersection provides a force due to SRP).

Since the spacecraft model is made up of small flat plates, the surface normal vector on the spacecraft at the point of intersection can be computed, and the flat-plate model can be used to compute the SRP forces.

Computing the SRP Force

At the point of intersection of each light ray with the spacecraft surface, the force due to SRP can be computed from Eq. (7) if the values for $Acos\theta$ and P_{SRP} are known.

The $Acos\theta$ term in Eq. (7) represents the area of the plate as seen by the Sun. Since each pixel on the array is projected onto the spacecraft from the Sun direction, the sum of all projected pixels (that make contact with the spacecraft) is approximately equal to the spacecraft area as seen by the Sun. This approximation improves with smaller chosen pixel size.

Thus, in SPAD, the $Acos\theta$ term in Eq. (7) is given by the pixel area (for a single pixel). Also, the Sun vector, $\hat{S}$, is given by the direction opposite the light-ray vector, and the surface-normal vector, $\hat{N}$, is found from the spacecraft surface model at the point of intersection.

In SPAD, the distance between the spacecraft and the Sun is not specified, and therefore P_{SRP} cannot be computed. To resolve this issue, SPAD instead computes $\vec{F}_{SRP}/P_{SRP}$ at each intersection using Eq. (7) (after dividing both sides by P_{SRP}). When this data is then fed into a trajectory propagation tool, P_{SRP} is computed and the force (and/or acceleration) due to SRP is calculated.

The SRP "force" equation used by SPAD is thus given by

$$\vec{F}_{SRP}/P_{SRP} = -A_{pixel}\left\{(1-C_s)\hat{S} + 2\left(C_s cos\theta + \frac{1}{3}C_d\right)\hat{N}\right\} \tag{10}$$

where A_{pixel} is the area of each pixel in the pixel array for the light-ray model, and θ is the angle between the known Sun-vector and surface-normal vector directions (computed at each intersection). The equation is used to compute the "force" (normalized by solar pressure) at each light-ray vector intersection with the spacecraft surface. The sum of the forces over all intersections represents the net SRP "force" acting on the spacecraft (for a particular specified orientation, i.e. azimuth and elevation angle). The process is then repeated for every spacecraft orientation specified by the user.

Choosing Modeling Parameters

To run the SRP analysis in SPAD, parameters must first be chosen, such as the number of reflections, the range and step size for azimuth and elevation angle, and the pixel size. For this analysis, we choose a 5° step size for both azimuth and elevation angle. To capture every orientation in discrete space, the range in azimuth goes from -180° to 180°, and the range in elevation goes from -90° to 90°. We note that in SPAD, elevation is measured with respect to the body-fixed x-y plane, and the azimuth is measured from the positive body-fixed x axis, in the direction of the positive y-axis (i.e. the angle measures a rotation about the positive z-axis).

The number of reflections that the user must choose in SPAD refers to the reflected light rays in the ray-tracing algorithm. SPAD can compute subsequent encounters of the light rays after reflecting off of the spacecraft surface. (We note that in SPAD, only the portion of light reflected *specularly* is considered for subsequent reflections.) To determine a meaningful number of reflections for this analysis, we run an SRP analysis in SPAD for reflection numbers ranging from 0 to 4. To keep the run time at a reasonable value (within a day), we set the azimuth and elevation

step size for these runs to 45 ^{o} and we set the pixel size to 0.02 m. The force values in the resulting output files showed no change beyond 2 reflections. Therefore, we use only 2 reflections in the final analysis.

The pixel size is determined in a similar fashion to that of the number of reflections. We run a SPAD analysis (using 2 reflections) for pixel sizes of 0.04 m, 0.02 m, 0.01 m, 0.005 m, and 0.0025 m. The resulting "force" (per unit P_{SRP}) values computed from Eq. (10) only changed by 0.01 m^2 (at most) from the 0.005 m and 0.0025 m analyses.

To help determine a meaningful pixel size, we consider the accuracy of the spacecraft model itself. The spacecraft model made in SPAD is not a perfect replica of OSIRIS-REx. For this analysis, we decided that such a precise model for the spacecraft is not necessary, and due to the limitations of the surface-generating tools in SPAD, is not feasible. In cases where components could not be modeled precisely, we adopted a "worst-case scenario" philosophy. Additionally, when small changes are made to the model (within the approximate tolerances of the model itself) the SPAD SRP analysis output is found to change on the order of 0.1 m^2. Thus, the only meaningful accuracy for the final SRP analysis (with the spacecraft model developed in SPAD) is within about 0.1 m^2. Using this as a guide, we found (by comparing SRP output from analyses with 0.02 m and 0.01 m pixel sizes) that a pixel size of 0.02 m is sufficient to maintain an accuracy on the order of 0.1 m^2.

SPAD SRP Force Computation Validation

We used the General Mission Analysis Tool (GMAT)[11] version R2014a to simulate the OSIRIS-REx trajectory during Orbit B. In order to have a benchmark for model validation, we considered two SRP models when propagating the orbit in GMAT: the SRP model from SPAD, and a cannonball SRP model. For all cases using the cannonball model, we use a C_R value of 1.4.

In addition to the two solar radiation forces, all GMAT simulations run in this study use a 16th-degree, 16th-order gravity model for Bennu, and account for 3rd body gravity perturbations from the Sun, Jupiter, Earth, Moon, Mars, and Venus. No extensive analysis was done in this study to determine which 3rd bodies to include in the model. The Sun and Jupiter are assumed to be the dominating perturbing 3rd bodies. The Earth, Moon, Mars, and Venus are also included due to their relatively close proximity to Bennu's orbit. We note that, other than SRP, no nongravitational forces (e.g. forces due to solar wind, spacecraft radiation, etc.) were modeled.

The two spacecraft orientations (nadir and Earth-pointing) are represented in GMAT using its built-in attitude model capabilities. These two models will be applied to the OSIRIS-REx orbit phase example that has been found to exhibit strong SRP force perturbations.

ORBIT STABILITY DESING USING ORBIT-AVERAGED VOP EQUATIONS

It has been found that, if a spacecraft is put into an orbit that is initially circular and over the terminator of an asteroid (i.e. orbit plane normal to the asteroid-to-Sun line), the effects of solar radiation pressure cause the orbit plane to shift and the eccentricity to vary over time. The goal of this work is to find a somewhat modified initial orbit geometry that minimizes these variations in orbit plane orientation and eccentricity: the resulting orbit will be referred to as *SRP-stable*. An

SRP-stable orbit has the properties that the secular change in eccentricity is ideally zero, and the precession rate of the orbit matches the asteroid orbital rate around the Sun, so keeping the spacecraft orbiting over the terminator. Similar work has been done in designing stable orbits for the OSIRIS-REx mission by modeling SRP as a potential function.[12]

In order to determine the geometry of an SRP-stable orbit, it is first necessary to derive expressions for the long-term effects of solar radiation pressure on the spacecraft orbit.

Assumptions

The following assumptions will be made for the purposes of this analysis.

- The orbit of the spacecraft about the asteroid is high enough that an inverse square law suffices for the asteroid gravity model. (For the case of OSIRIS-Rex Orbit B, the orbital radius is roughly equal to four asteroid radii, so this assumption is certainly valid.)
- The eccentricity of the spacecraft orbit about the asteroid is small enough that first-order modeling of eccentricity effects is valid.
- The spacecraft is in a near-terminator orbit about the asteroid.
- The spacecraft has a constant ratio of projected area to the Sun and mass, and behaves as a pure solar absorber.
- The changes in the spacecraft orbital elements that are caused by solar radiation pressure occur slowly enough that integration over a complete spacecraft orbit, using constant element values in the VOP equations across this range, is valid.

Geometry of Near-Terminator Orbit

For a terminator orbit, the spacecraft orbit normal is ideally aligned with the vector from the center of the asteroid to the center of the Sun (or the negative of this vector: the choice depends on whether the spacecraft orbits the asteroid counter-clockwise or clockwise as viewed from the Sun). In reality, the orbit normal will be offset somewhat from this vector, with the offset evolving slowly with time as a result of orbital perturbations. This offset can be described by the following two angles: the first is the angle λ between the asteroid-to-Sun vector, $\hat{\mathbf{s}}$, and the spacecraft orbit normal, $\hat{\mathbf{h}}$,

$$\lambda = \text{acos}(\hat{\mathbf{s}}^T \hat{\mathbf{h}}). \tag{11}$$

The second angle required, denoted by ψ, is that between the projection of $\hat{\mathbf{s}}$ onto the spacecraft orbit plane and the spacecraft periapse vector, $\hat{\mathbf{P}}$. (We note that, although the spacecraft orbit is near-circular, it will not be precisely circular; $\hat{\mathbf{P}}$ will therefore be defined.) The projection of $\hat{\mathbf{s}}$ onto the orbit plane is given as

$$\mathbf{s}_{proj} = \hat{\mathbf{s}} - (\hat{\mathbf{s}}^T \hat{\mathbf{h}})\hat{\mathbf{h}}, \tag{12}$$

which when normalized, gives ψ (without quadrant ambiguity), in terms of the components of $\hat{\mathbf{s}}_{proj}$ along the perifocal frame vectors $\hat{\mathbf{P}}$ and $\hat{\mathbf{Q}}$ as

$$\cos\psi = \hat{\mathbf{P}}^T \hat{\mathbf{s}}_{proj},$$
$$\sin\psi = \hat{\mathbf{Q}}^T \hat{\mathbf{s}}_{proj}. \tag{13}$$

Solar Radiation Acceleration Vector

A coordinate system that is often used for orbital perturbation studies is the satellite local radial, tangential, orbit-normal rotating frame, termed the *RSW* frame:[8] the *R*-axis is directly radially outwards, *W* along the orbit angular momentum, and *S* along the forward tangent, completing a right-handed triad. The angles λ and ψ can now be used to express the RSW components of the acceleration vector that acts on the spacecraft as a result of SRP, in order to be able to apply it to the Gaussian Variation of Parameter (VOP) equations. The SRP acceleration vector is

$$\mathbf{a} = -p_s (A/m)\hat{\mathbf{s}}, \tag{14}$$

where A is the projected area of the spacecraft to the Sun, m its mass, and p_s the solar radiation pressure.

The components of the SRP acceleration vector in this frame can be expressed as follows. The component along the fixed out-of-plane (*W*) axis is simply given as

$$\mathrm{a}_W = \mathbf{a}^T \hat{\mathbf{h}} = -p_s (A/m)\cos\lambda. \tag{15}$$

The expressions for the components along the rotating *R* and *S* axes are somewhat more complicated. The vectors $\hat{\mathbf{R}}$ and $\hat{\mathbf{S}}$ are related to the perifocal frame axes $\hat{\mathbf{P}}$ and $\hat{\mathbf{Q}}$ as

$$\hat{\mathbf{R}} = \cos\nu\,\hat{\mathbf{P}} + \sin\nu\,\hat{\mathbf{Q}},$$
$$\hat{\mathbf{S}} = -\sin\nu\,\hat{\mathbf{P}} + \cos\nu\,\hat{\mathbf{Q}}. \tag{16}$$

Using these and Eqs. (13) then gives the desired components as

$$\mathrm{a}_R = -p_s (A/m)\sin\lambda\cos(\nu - \psi),$$
$$\mathrm{a}_S = p_s (A/m)\sin\lambda\sin(\nu - \psi). \tag{17}$$

Solar Radiation-Induced Orbit-Averaged VOP Expressions

The effect of perturbation accelerations on the spacecraft orbit about the asteroid can be studied efficiently using the Variation of Parameters equations:[13] these describe the changes in the orbital elements that are produced by small perturbation accelerations as a function of where on the orbit they act. The Gaussian form of the first five of these equations can be written in terms of the perturbation acceleration vector when this is expressed as its components in the RSW frame.[8] The resulting VOP equations are then

$$\dot{a} = \frac{2}{n\sqrt{1-e^2}}\left[e\sin\nu\,\mathrm{a}_R + (1+e\cos\nu)\,\mathrm{a}_S\right], \tag{18}$$

$$\dot{e} = \frac{\sqrt{1-e^2}}{na}\left[\sin\nu\,\mathrm{a}_R + \frac{(e+2\cos\nu+e\cos^2\nu)}{(1+e\cos\nu)}\mathrm{a}_S\right], \tag{19}$$

$$\dot{i} = \frac{r\cos(\omega+\nu)}{na^2\sqrt{1-e^2}}\mathrm{a}_W, \tag{20}$$

$$\dot{\Omega} = \frac{r\sin(\omega+\nu)}{na^2\sqrt{1-e^2}\sin i}\mathrm{a}_W \tag{21}$$

and

$$\dot{\omega} = \frac{\sqrt{1-e^2}}{nae}\left[-\cos\nu\,\mathrm{a}_R + \sin\nu\frac{(2+e\cos\nu)}{(1+e\cos\nu)}\mathrm{a}_S - \frac{e\cot i\sin(\omega+\nu)}{(1+e\cos\nu)}\mathrm{a}_W\right]. \tag{22}$$

A corresponding equation also exists for the mean anomaly at epoch, M_0, serving to describe how the phasing of the satellite is affected by the perturbations. However, the precise phasing of the spacecraft need not be characterized in order to calculate the desired stable orbit about an asteroid in the face of SRP effects. Therefore, this sixth VOP equation is not required.

The right-hand sides of Eqs. (18-22) involve the instantaneous values of the orbital elements, and are exact expressions. However, if the applied perturbations are small, the changes in the elements over a single spacecraft orbit will also be relatively small, which permits the simplification of holding the values constant while evaluating the VOP expressions over each rev. The resulting "orbit-averaged" values for the changes in each element are approximations, but are close to the true values for small perturbations, as is the case here. We note that the well-known secular oblateness-induced rates of change of the right ascension of the ascending node (RAAN) and argument of perigee (AOP) are derived[14] using orbit-averaging of the VOP equations, with the applied perturbation acceleration components in this case being those produced by the J_2 term in the Earth gravity harmonic expansion.

As an example, the orbit-averaged change in semi-major axis (SMA) will now be derived, which will also serve to show a detail that is involved. This detail is the fact that Eq. (18) gives the time rate of change of SMA in terms of true anomaly, not time. Integrating Eq. (18) over one rev to find Δa_{rev} therefore requires the change of variables

$$\Delta a_{rev} = \int_0^T \dot{a}dt = \int_0^{2\pi} \dot{a}(\nu)\frac{dt}{d\nu}d\nu = \int_0^{2\pi} \left[\dot{a}(\nu)/\dot{\nu}\right]d\nu\,. \tag{23}$$

But the angular momentum of the spacecraft orbit can be expressed in two forms, as

$$h = \dot{\nu}r^2 = \sqrt{\mu p}\,, \tag{24}$$

where μ is the gravitational parameter of the asteroid, which then implies that

$$\dot{\nu} = \frac{h}{r^2} = \frac{\sqrt{\mu p}}{p^2}(1+e\cos\nu)^2 = \sqrt{\frac{\mu}{p^3}}(1+e\cos\nu)^2\,. \tag{25}$$

For orbits with small eccentricity, as assumed here, the binomial expansion can be used to approximate $\dot{\nu}$ as

$$\dot{\nu} \approx \sqrt{\frac{\mu}{p^3}}(1-2e\cos\nu) \tag{26}$$

Now, combining Eqs. (17) and (18) gives the following expression for $\dot{a}$:

$$\dot{a} = \frac{2}{n\sqrt{1-e^2}} p_s (A/m) \sin\lambda \left[-e \sin\nu \cos(\nu - \psi) + (1 + e\cos\nu)\sin(\nu - \psi) \right], \tag{27}$$

which can be rearranged to give

$$\dot{a} = c_a \left[\sin(\nu - \psi) - e\sin\psi \right] = c_a \left[\sin\nu\cos\psi - (e + \cos\nu)\sin\psi \right], \tag{28}$$

where

$$c_a = \frac{2}{n\sqrt{1-e^2}} p_s (A/m) \sin\lambda. \tag{29}$$

Substituting Eq. (29) and Eq. (26) into Eq. (23) then gives

$$\Delta a_{rev} \approx c_a \sqrt{p^3/\mu} \cdot \int_0^{2\pi} \left[\sin\nu\cos\psi - (e + \cos\nu)\sin\psi \right] (1 - 2e\cos\nu) d\nu. \tag{30}$$

Expanding the terms that make up the integrand gives expressions of the form $\sin\nu$, $\cos\nu$ and $\sin\nu\cos\nu$, all of which integrate to zero over a complete rev. The only terms that do not individually yield zero give

$$\begin{aligned} \Delta a_{rev} &\approx c_a \sqrt{p^3/\mu} \cdot \int_0^{2\pi} \left[-e\sin\psi (1 - 2\cos^2\nu) \right] d\nu \\ &= c_a \sqrt{p^3/\mu} \cdot \left[-e\sin\psi (2\pi - 2\pi) \right] = 0. \end{aligned} \tag{31}$$

No secular drift in semi-major axis should therefore be produced by solar radiation pressure. This observation makes sense: the in-plane component of the SRP perturbation is essentially inertially fixed, and so its effect on SMA cancels over the course of a complete rev.

Using similar methods, the net change in eccentricity that is produced by the SRP perturbation over one spacecraft rev can be shown to be

$$\Delta e_{rev} = -3\pi \frac{(1-e^2)^3 a^2}{\mu} p_s (A/m) \sin\lambda \sin\psi. \tag{32}$$

Likewise, the orbit-averaged change in inclination over one rev is given as

$$\Delta i_{rev} = 3\pi \frac{(1-e^2)^2 a^2}{\mu} p_s (A/m) e \cos\lambda \cos\omega, \tag{33}$$

the change in RAAN is

$$\Delta\Omega_{rev} = 3\pi \frac{(1-e^2)^2 a^2}{\mu} p_s (A/m) e \operatorname{cosec} i \cos\lambda \sin\omega, \tag{34}$$

and finally the change in AOP is

$$\Delta\omega_{rev} = 3\pi \frac{(1-e^2)^2 a^2}{\mu e} p_s (A/m) \left[\sin\lambda\cos\psi - e^2 \cot i \cos\lambda \sin\omega \right]. \tag{35}$$

Application to SRP-Stable Terminator Orbit Design

These integrated VOP equations can now be used to design a terminator orbit around an asteroid that, as much as possible, remains a terminator orbit of fixed size and shape for an extended period, despite the presence of SRP perturbations. We refer to such an orbit as SRP-stable (which is equivalent to the frozen orbits of Ref. 12). To remain over the terminator, Ω for the orbit must increase at an average rate equal to the mean motion of the asteroid around the Sun, n_{ast}. For the orbit geometry to remain fixed, the averaged rates of change of the remaining elements *a*, *e*, *i* and ω must be small. We see from Eq. (31) that the change in SMA is indeed zero, and we must design the orbit to give zero rates for *e*, *i* and ω (i.e. zero values for the average changes expressed in Eqs. (32), (33), and (35)).

This problem is simpler to describe if the elements of the spacecraft orbit are defined relative to the orbital plane of the asteroid around the Sun rather than in terms of the Ecliptic plane. In this coordinate system, the inclination that is required for a terminator orbit is *i* = 90 deg (putting the spacecraft orbit normal in the asteroid orbital plane); in addition, the angle λ that is defined by Eq. (11) must be either zero (motion counter-clockwise as viewed from the Sun) or 180 deg (clockwise). Since we then have that $\sin\lambda = 0$, Eq. (32) implies that $\Delta e_{rev} = 0$, as desired. (We note that, if an orbit is allowed to slip out of terminator conditions, e.g. by not achieving the desired average nodal drift rate, eccentricity will change over time, which will be illustrated by numerical results later in the paper.) Similarly, substituting *i* = 90 deg and $\sin\lambda = 0$ into Eq. (35) gives $\Delta\omega_{rev} = 0$, again as desired.

The only two remaining averaged rates that must be considered are therefore those of inclination and RAAN, which become

$$\Delta i_{rev} = \pm 3\pi \frac{(1-e^2)^2 a^2}{\mu} p_s (A/m) e \cos\omega, \tag{36}$$

and

$$\Delta\Omega_{rev} = \pm 3\pi \frac{(1-e^2)^2 a^2}{\mu} p_s (A/m) e \sin\omega; \tag{37}$$

the sign variability arises from the fact that $\cos\lambda = \pm 1$. In order to have $\Delta i_{rev} = 0$ while having a non-zero $\Delta\Omega_{rev}$, we must clearly select that $\cos\omega = 0$, i.e. ω is either 90 or 270 deg. Furthermore, in order to ensure that $\Delta\Omega_{rev}$ is positive, we must select ω = 90 deg if λ = 0, and ω = 270 deg if λ = 180 deg. The resulting net change in RAAN over the course of one spacecraft orbit is then

$$\Delta\Omega_{rev} = 3\pi \frac{(1-e^2)^2 a^2}{\mu} p_s (A/m) e \approx 3\pi \frac{a^2}{\mu} p_s (A/m) e, \tag{38}$$

to first order in the small parameter *e*. However, for the orbit to remain over the terminator, we require that the orbit precess in step with the motion of the asteroid around the Sun. We therefore require that

$$\Delta\Omega_{rev} = n_{ast} T = 2\pi n_{ast} \sqrt{a^3/\mu}. \tag{39}$$

Rearranging Eq. (29) gives the value of eccentricity of the spacecraft orbit that achieves this condition

$$e^* = \frac{2}{3} \cdot \frac{n_{ast}\, \mathrm{v}_{orb}}{p_s (A/m)}, \tag{40}$$

where $\mathrm{v}_{orb} = \sqrt{\mu/a}$ is the circular orbit speed of the spacecraft relative to the asteroid. The physical mechanism by which the terminator orbit condition is maintained by this small initial eccentricity is as follows: if the orbit were circular, the out-of-plane acceleration produced by SRP would average to zero over the course of a complete rev. For a non-zero eccentricity, however, there will effectively be an unbalanced out-of-plane Δv at apoapsis; if the apoapsis is positioned midway between the nodes (i.e. for ω either 90 or 270 deg), the effect of this Δv will be to shift the position of the nodes, as desired.

OSIRIS-REx ORBIT B EXAMPLE: ANALYSIS AND SIMULATION RESULTS

Orbit B

The OSIRIS-REx spacecraft is inserted into an orbit about Bennu (called Orbit B) approximately 3.5 years after launch, and remains in this orbit for about 60 days. Orbit B is the seventh phase of the mission and is key for the success of sample retrieval. The primary activity of OSIRIS-REx during Orbit B is to gather optical data for 12 potential touch-and-go (TAG) sample collection sites at 5 cm resolution, and to perform high fidelity mapping of Bennu's gravity field. The nominal Orbit B trajectory is a near-circular 1-km orbit about Bennu with a period of approximately 27 days, and is oriented about Bennu such that the orbit normal is parallel to the Bennu-Sun direction (i.e. a terminator orbit).

To help describe the spacecraft attitude, the body-fixed axes are defined as shown in Figure 5. In the figure, the solar arrays and high-gain antenna (HGA) are directed along the +x direction, and the Touch-And-Go Sample Acquisition Mechanism (TAGSAM) extends along the +z direction. The +y direction is defined to complete the triad. We note that, contrary to what is shown in the figure, the TAGSAM will be in its stowed position when orbiting Orbit B.

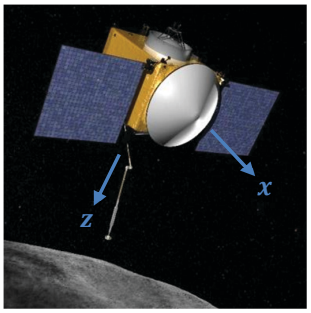

Figure 5. OSIRIS-REx spacecraft with body-fixed axes shown. In the nominal orientation during Orbit B, the x-axis points toward the Sun, and the z axis points toward Bennu (i.e. is nadir). This figure has been adapted from an image at www.nasa.gov.

To keep the solar panels in the path of direct sunlight, as well as to collect data, the nominal attitude of the spacecraft is nadir pointing with the +z axis always pointing towards Bennu, and the +x axis always pointing towards the Sun. Every 24 hours however, the spacecraft must change its orientation and point the high-gain antenna (HGA), i.e. the +x axis, toward Earth to transmit the collected data. Therefore, every 24 hours in Orbit B (for the simulations run in this study), OSIRIS-REx spends 16 hours in the nominal nadir orientation, and 8 hours in the Earth-pointing orientation. For this investigation, the 24-hour cycle repeats for about 60 days (the entirety of Orbit B). More detailed illustrations of OSIRIS-REx's two orientations during Orbit B are shown in Figure 6.

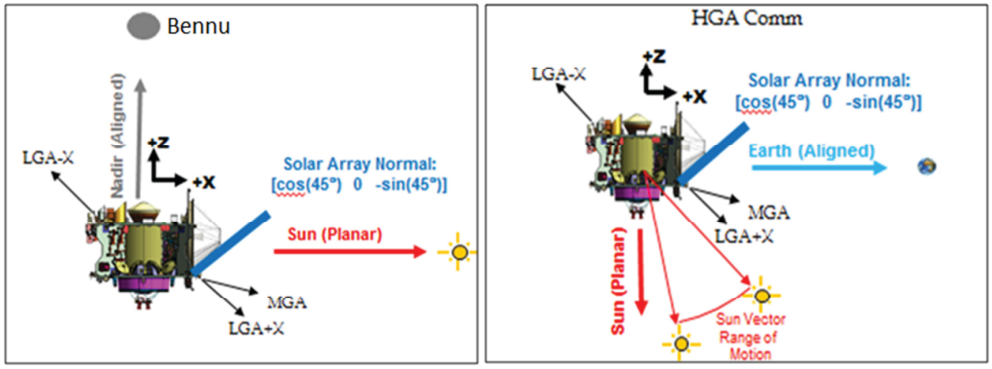

(a) **(b)**

Figure 6 Nominal, nadir-pointing OSIRIS-REx orientation (a), and HGA Earth-pointing orientation (b) during Orbit B.[1]

We note that it is evident that the attitude changes affect the SPAD designed SRP model, but not the cannonball model (which assumes the spacecraft is a perfect sphere).

SRP-Stable Orbit B

In this section, we present the analysis and comparisons of the cannonball SRP model to the high fidelity SPAD SRP model in designing a stable orbit.

Equation (40) yields an SRP-stable orbital eccentricity value e^* of 0.139, using the following numerical values that correspond to OSIRIS-Rex Orbit B:

- Spacecraft mass (during Orbit B): mass = 1,198 kg
- Spacecraft projected area: $A = 12$ m^2
- Spacecraft coefficient of reflectivity: $c_r = 1.4$
- Bennu gravitational parameter: $\mu = 4.16$ km^3/s^2
- Spacecraft-orbit semi-major axis (about Bennu): a = 1,000 m (4 times asteroid radius of ~250 m)
- Spacecraft mean orbital speed: $v_{orb} = 0.06450$ m/s
- Bennu's mean motion (heliocentric): $n = 1.67\text{x}10^{-7}$ rad/s
- Bennu's solar distance: 1.11 AU
- SRP: $p_s = 3.69\text{x}10^{-6}$ N/m^2

The corresponding spacecraft apoapse and periapse radii are 1,139 m, and 861 m, respectively.

Orbit B Simulation using Cannonball SRP Model

The stability of the modified Orbit B design was tested in GMAT using both the lower-fidelity cannonball SRP model, and the high-fidelity SRP model from SPAD. In this section, the results from the cannonball SRP model are investigated. (The SPAD SRP model is investigated in the next section.) The other forces modeled in the GMAT simulation are described in the Methods section.

The results are shown in Figures 7 and 8. Figure 7 shows the trajectory in the Bennu-Sun rotating frame, where the view is along the Bennu-Sun direction. In this view, an un-perturbed terminator orbit would appear as a single circle or ellipse. The yellow arcs shown in Figure 7 represent times when the spacecraft is in its nadir-pointing orientation (16 hrs per day), and the blue arcs represent times when the spacecraft is oriented with its HGA directed at Earth (8 hrs per day). For a spherical spacecraft however, the orientation changes make no impact on the SRP force or the trajectory.

Figure 7a shows the propagated Orbit B trajectory using the nominal initial orbit conditions (with $e = 0$), and Figure 7b shows the Orbit B propagation with the redesigned orbit ($e = e^* = 0.139$). We note that this result is in close agreement with the frozen orbit condition of Ref. 12, which was derived using different methods than the Gaussian VOP approach used here. Over the 60-day propagation, both trajectories exhibit perturbation; however, the redesigned trajectory in Figure 7b is clearly improved.

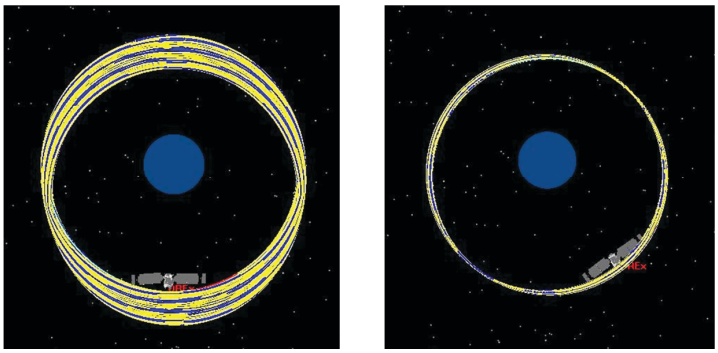

(a) **(b)**

Figure 7. GMAT propagation of Orbit B using a cannonball SRP model for (a) the nominal Orbit B trajectory initial conditions, and (b) the redesigned, SRP-stable, Orbit B initial conditions (with $e = e^*$).

Figure 8 shows these differences more clearly, by plotting the time history of Ω, λ, and e over the 60-day propagation. The plot shows that, compared to the nominal Orbit B propagation (blue), the redesigned Orbit B (green) has an Ω that precesses at nearly a constant rate (as desired in order to follow the orbit of Bennu about the Sun), which results in about a 4° reduction in the maximum deviation of λ. The amplitude of eccentricity change for the redesigned Orbit B reduced to about one-fifth that of the nominal. The results shown in red represent an attempt (via

trial-and-error) to improve upon the designed e^*. The results in Figure 8 show only small improvements (if any) from this attempt over the VOP derived e^* results.

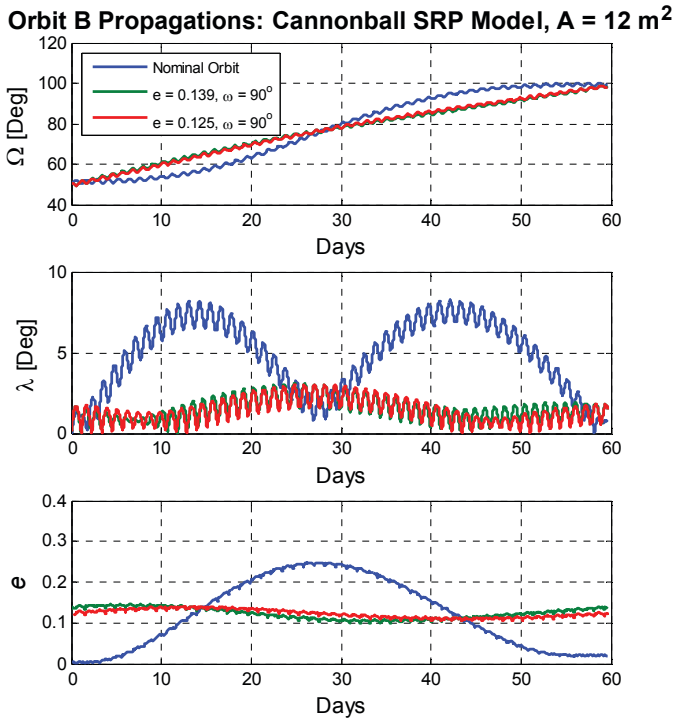

Figure 8. Time history of Ω, λ, and e over a 60-day GMAT propagation of Orbit B using the cannonball SRP model. The nominal trajectory is shown in blue, the designed orbit ($e = e^*$) is shown in green, and an attempt at improving the designed e^* (via trial-and-error) is shown in red.

Orbit B Simulation using High-Fidelity SPAD SRP Model

In the design of the stabilized Orbit B we assumed a cannonball-SRP model, which was investigated in the previous section. In this section, the redesigned Orbit B is investigated in high-fidelity, by propagating the Orbit B trajectory in GMAT using the SPAD SRP model.

Figure 9 shows the trajectory in the Bennu-Sun rotating frame (similar to that of Figure 7), where the view is along the Bennu-Sun direction. The propagation of the Orbit B trajectory using the nominal initial orbit conditions (with $e = 0$) is shown in Figure 9a and the propagation of the stabilized Orbit B (with $e = e^* = 0.139$) is shown in Figure 9b. Both trajectories are clearly perturbed; however, the designed trajectory in Figure 9b exhibits less perturbation over the 60-day simulation. The yellow arcs shown in Figure 9 represent times when the spacecraft is in its nadir-pointing orientation, and the blue arcs represent times when the spacecraft is oriented with its HGA directed at Earth. Unlike with the cannonball SRP model, however, the orientation changes do have an impact on the SRP force, and thus, the resulting propagation of Orbit B.

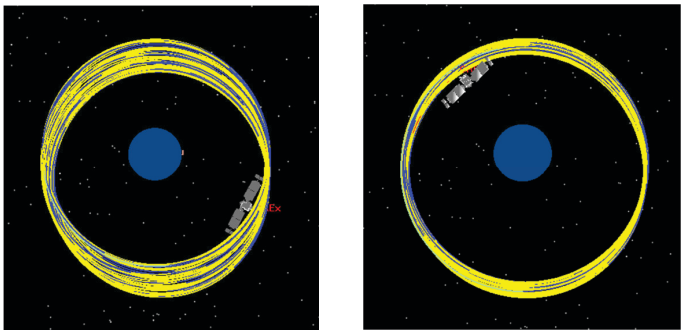

(a) **(b)**

Figure 9. High-fidelity GMAT propagation of Orbit B using the SPAD SRP model for (a) the nominal Orbit B trajectory initial conditions, and (b) the redesigned, SRP-stable Orbit B initial conditions (with $e = e^*$).

Figure 10 shows the time history of Ω, λ, and e over the 60-day propagation, for the nominal Orbit B propagation (blue), the stabilized Orbit B with $e = e^*$ (green), and a propagation using a modified eccentricity (red) found via trial and error. Compared to the nominal Orbit B propagation, the stabilized Orbit B has an Ω that precesses at an approximately constant rate, which reduces the maximum deviation of λ by about 5°. The amplitude of eccentricity change for the stabilized Orbit B is also reduced to about one-half that of the nominal. The results shown in red, for the propagation using modified eccentricity (found via trial and error), show little to no improvement over green results (with the VOP-derived e^*).

Upon examination of λ, and e in Figures 8 and 10, the behavior observed in Fig. 10 is less predictable than that observed in Fig. 8. This difference in behavior can be attributed to the relatively large variations in SRP force acting on the spacecraft when the high-fidelity SRP model is used versus the cannonball model. As light hits the OSIRIS-REx model (shown in Fig. 3), the changes in the spacecraft attitude result in changes in the direction of the reflected light (which does not occur for the cannonball SRP model). Additionally, as the spacecraft changes its attitude, the surfaces on the spacecraft that are visible to the sun can change, which may have different surface properties from those previously in view. These changes in surface properties will result in further deviations between the high-fidelity SRP model results versus the results found using the cannonball model (which assumes uniform surface properties). Overall, the asymmetry of the spacecraft's shape in the high-fidelity model drives the solution's unpredictable behavior in Fig. 10. The perfectly spherical spacecraft assumed for the cannonball SRP model has constant SRP forces regardless of the spacecraft's orientation: allowing the precession rate of the orbit to smoothly oscillate about the target precession rate (i.e. the rate to maintain the terminator orbit), which (for a spherical spacecraft) results in the smooth oscillation of the eccentricity (as shown in Fig. 8).

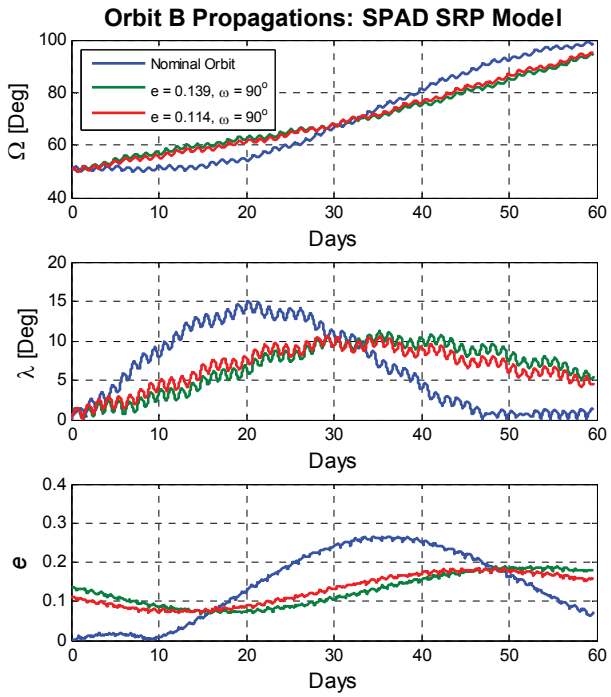

Figure 10. Time history of Ω, λ, and e over the 60-day GMAT propagation of Orbit B, using the SPAD SRP model. The nominal trajectory is shown in blue, the designed orbit ($e = e^*$) is shown in green, and an attempt at improving the designed e^* (via trial and error) is shown in red.

CONCLUSION

For OSIRIS-REx, understanding the trajectory perturbations due to SRP is essential for the success of its mission. By modifying the eccentricity of the spacecraft's orbit about Bennu, the resulting trajectory thereafter remains much closer to the nominal terminator orbit (compared to that of the nominal Orbit B with $e = 0$). Furthermore, the variations in eccentricity over the 60-day simulation were shown to reduce in amplitude by a factor of five for the case of the cannonball SRP model, and by a factor of two for the case of the high-fidelity SRP model. Maintaining orbit stability through the implementation of simple, passive orbit modifications (such as the one presented in this paper) may prove key to maintaining such stability with very little impact on mission cost.

REFERENCES

[1] Lauretta D.S., "An Overview of the OSIRIS-REx Asteroid Sample Return Mission," 43rd Lunar Planetary Science Conference, 2012.

[2] Lauretta, D.S., Bartels, A.E., Barucci, M.A., Bierhaus, E.B., Binzel, R.P., Bottke, W.F., Campins, H., Chesley, S.R., Clark, B.C., Clark, B.E., Cloutis, E.A., Connolly, H.C., Crombie, M.K., Delbo, M., Dworkin, J.P., Emery, J.P., Glavin, D.P., Hamilton, V.E., Hergenrother, C.W.,

Johnson, C.L., Keller, L.P., Michel, P., Nolan, M.C., Sandford, S.A., Scheers, D.J., Simon, A.A., Sutter, B.M., Vokrouhlicky, D., and Walsh, K.J., "The OSIRIS-REx Target Asteroid (101955) Bennu: Constraints on its Physical Geological, and Dynamical Nature from Astronomical Observations," *Meteoritics and Planetary Science*, Vol. 50, No. 4, pp. 834–849, 2015.

[3] Longuski, J.M., Todd, R.E., and König, W.W., "Survey of Nongravitational Forces and Space Environment Torques: Applied to the Galileo," *Journal of Guidance, Control, and Dynamics*, Vol. 15, No. 3, May–June 1992, pp. 545–553.

[4] Lambert, J.H., *Photometria: Sive de Mensura et Gradibus Luminis, Colorum et Umbrae*, 1760.

[5] Ziebart, M., "Generalized Analytical Solar Radiation Pressure Modeling Algorithm for Spacecraft of Complex Shape," *Journal of Spacecraft and Rockets*, Vol. 41, No. 5, Sept.–Oct. 2004, pp. 840–848.

[6] Georgevic, R.M., "Mathematical Model of the Solar Radiation Forces and Torques Acting on the Components of a spacecraft," NASA TM-JPL-33-494, Oct. 1971.

[7] Wertz, J. (ed), *Spacecraft Attitude Determination and Control*, Microcosm, Torrance, CA, 1978.

[8] Vallado, D. A., *Fundamentals of Astrodynamics and Applications*, Third Edition, Hawthorne, CA, Microcosm Press, and New York, NY, Springer, 2007.

[9] Olds, R., "Surface Property Data for Solar Radiation Pressure Modeling," NASA-GSFC Technical Memo, NFP3-AC-13-0022, October 15, 2013.

[10] Ziebart. M., and Dare.P., "Analytical solar radiation pressure modeling for GLONASS using a pixel array," *Journal of Geodesy,* (2001) 75: 587-599.

[11] Hughes, S.P., Qureshi, R.H., Cooley, D.S., Parker, J.K., and Grubb, T.G., "Verification and Validation of the General Mission Analysis Tool (GMAT)," AIAA Paper No. 2014-4151, AIAA/AAS Astrodynamics Specialist Conference, San Diego, CA, Aug. 4–7, 2014.

[12] Scheeres, D.J., Sutter, B.M., and Rosengren, A.J., "Design, Dynamics and Stability of the OSIRIS-REx Sun-Terminator Orbits," *23rd AAS/AIAA Space Flight Mechanics Conference*, Kauai, Hawaii, February 2013.

[13] Bate, R.R., Mueller, D.D., and White, J.E., *Fundamentals of Astrodynamics*, Dover Publications, 1971.

[14] Prussing, J.E. , and Conway, B.A., *Orbital Mechanics*, Oxford University Press, 1993.